J. Fluid Mech. (2004), *vol.* 515, *pp.* 293–317.
DOI: 10.1017/S0022112004000370 Printed in the United Kingdom

A diffuse-interface method for simulating two-phase flows of complex fluids

By PENGTAO YUE[1], JAMES J. FENG[1], CHUN LIU[2] AND JIE SHEN[3]

[1]Department of Chemical and Biological Engineering and Department of Mathematics, University of British Columbia, Vancouver, BC V6T 1Z4, Canada

[2]Department of Mathematics, The Pennsylvania State University, University Park, PA 16802, USA

[3]Department of Mathematics, Purdue University, West Lafayette, IN 47907, USA

(Received 10 November 2003 and in revised form 7 May 2004)

Two-phase systems of microstructured complex fluids are an important class of engineering materials. Their flow behaviour is interesting because of the coupling among three disparate length scales: molecular or supra-molecular conformation inside each component, mesoscopic interfacial morphology and macroscopic hydrodynamics. In this paper, we propose a diffuse-interface approach to simulating the flow of such materials. The diffuse-interface model circumvents certain numerical difficulties in tracking the interface in the classical sharp-interface description. More importantly, our energy-based variational formalism makes it possible to incorporate complex rheology easily, as long as it is due to the evolution of a microstructure describable by a free energy. Thus, complex rheology and interfacial dynamics are treated in a unified framework. An additional advantage of our model is that the energy law of the system guarantees the existence of a solution. We will outline the general approach for any two-phase complex fluids, and then present, as an example, a detailed formulation for an emulsion of nematic drops in a Newtonian matrix. Using spectral discretizations, we compute shear-induced deformation, head-on collision and coalescence of drops where the matrix and drop phases are Newtonian or viscoelastic Oldroyd-B fluids. Numerical results are compared with previous studies as a validation of the theoretical model and numerical code. Finally, we simulate the retraction of an extended nematic drop in a Newtonian matrix as a method for measuring interfacial tension.

1. Introduction

Complex fluids are those with internal microstructures whose evolution affects the macroscopic dynamics of the material, especially the rheology. Examples include polymer solutions and melts, liquid crystals, gels, suspensions, emulsions and micellar solutions (Larson 1999). Such materials often have great practical utility since the microstructure can be manipulated via processing the flow to produce useful mechanical, optical or thermal properties. An important way of utilizing complex fluids is through composites. By blending two immiscible components together, one may derive novel or enhanced properties from the composite, and this is often a more economical route to new materials than synthesis. Moreover, the properties of composites may be tuned to suit a particular application by varying the composition, concentration and, most importantly, the *phase morphology*. Perhaps the most important of such

composites are polymer blends (Utracki 1990). Under optimal processing conditions, the dispersed phase is stretched into a fibrillar morphology. Upon solidification, the long fibres act as *in situ* reinforcement and impart great strength to the composite. The effect is particularly strong if the fibrillar phase is a liquid-crystalline polymer (LCP) (National Research Council 1991). Another example is polymer-dispersed liquid crystals (PDLCs), with liquid crystal droplets embedded in a polymer matrix, which have shown great potential in electro-optical applications (West 1990).

From a fundamental viewpoint, such composites are extremely interesting. They feature dynamic coupling of three disparate length scales: molecular or supra-molecular conformation inside each component, mesoscopic interfacial morphology and macroscopic hydrodynamics. The complexity of such materials has for the most part prohibited theoretical and numerical analysis. The main difficulty is the moving and deforming interface between the two components. The material thus has myriad internal boundaries. Traditional fluid dynamics treats these as sharp interfaces on which matching conditions must be imposed. This leads to an almost intractable theoretical problem. A secondary difficulty is that the rheology of each component alone is highly complex, with the internal microstructure coupled with the flow field.

A conceptually straightforward way of handling the moving interfaces is to employ a mesh that has grid points on the interfaces, and deforms according to the flow on both sides of the boundary. This has been implemented in boundary integral and boundary element methods (Cristini, Blawzdziewicz & Loewenberg 1998; Toose, Geurts & Kuerten 1995; Khayat 2000), finite-element methods (Hu, Patankar & Zhu 2001; Ambravaneswaran, Wilkes & Basaran 2002; Hooper *et al.* 2001*a*, *b*; Kim & Han 2001) and a finite-difference method (Ramaswamy & Leal 1999*a*, *b*). Keeping track of the moving mesh entails a large computational overhead. Furthermore, large displacement of internal domains causes mesh entanglement as happens, say, when one drop overtakes another. Typically, a remeshing scheme is activated, introducing interpolation error as well as additional computational cost. Most importantly, the moving-mesh methods cannot handle singular morphological changes such as breakup, coalescence and reconnection; the sharp interface formulation breaks down in such events. Thus, these methods have been limited mostly to single drops undergoing relatively mild deformations.

As an alternative, fixed-grid methods that regularize the interface have been highly successful in treating deforming interfaces. These include the volume-of-fluid (VOF) method (Li & Renardy 2000*a*), the front-tracking method (Unverdi & Tryggvason 1992) and the level-set method (Chang *et al.* 1996). Instead of formulating the flow of two domains separated by an interface, these methods represent the interfacial tension as a body force or bulk stress spread over a narrow region covering the interface. Then a single set of governing equations can be written over the entire domain, and solved on a fixed grid in a purely Eulerian framework. So far, the application of these methods has been mostly limited to Newtonian fluids. The only departure from Newtonian rheology appears to be an effort to introduce a yield stress to the continuous phase (Li & Renardy 2000*b*). See Sethian & Smereka (2003) for an insightful comparison of these methods.

The diffuse-interface model can be viewed as a physically motivated level-set method. Instead of choosing an artificial smoothing function for the interface, which affects the results in non-trivial ways if the radius of interfacial curvature approaches that of the interfacial thickness (Lowengrub & Truskinovsky 1998), the diffuse-interface model describes the interface by a mixing energy. This idea can be traced to van der Waals (1892), and is the foundation for the phase-field theory for phase

transition and critical phenomena (Hohenberg & Halperin 1977). Thus, the structure of the interface is determined by molecular forces; the tendencies for mixing and demixing are balanced through the non-local mixing energy. When the capillary width approaches zero, the diffuse-interface model becomes identical to a sharp-interface level-set formulation. It also reduces properly to the classical sharp-interface model.

Notwithstanding its physical root, we use the diffuse-interface method mainly as a numerical technique for handling morphological changes of the interfaces. The main attraction for us is its capability to easily incorporate the complex rheology of microstructured fluids. This is by virtue of its energy-based variational formalism. The conformation of the microstructure is often governed by a free energy, e.g. the Frank distortion energy for a liquid crystal or the free energy of a polymer chain. This can be added to the mixing energy to form the total free energy of the multi-phase system. Then the formal variational procedure applied on the total free energy will give rise to the proper constitutive equation for the microstructured fluids in addition to the evolution equation of the phase field variable. Thus, interfacial dynamics and complex rheology are included in a unified theoretical framework. Dissipative effects such as viscous stresses, of course, have to be accounted for separately, e.g. via the standard irreversible thermodynamic procedure (Lowengrub & Truskinovsky 1998) or by including Brownian motion in Hamilton's principle (Peskin 1985; Gliklikh 1997).

An additional advantage of the diffuse-interface method over other interface-regularizing methods is its energy conservation. Lin & Liu (1995, 2000) have rigorously proved that this ensures the existence of classical and finite-dimensional weak solutions for the system, the latter including numerical approximations by, e.g., finite-element and spectral methods. In VOF simulations, density is the labelling function subjected to smoothing. The level-set method renormalizes the distance function. In either case, the conservation of energy cannot be maintained. When the geometry is simple and the solution is smooth, non-conservation of energy usually does not compromise the quality of the solution. But difficulties may arise in the presence of rapid spatial variations, which are characteristic of microstructured fluids with internal boundaries and/or defects (Larson 1999).

As alluded to before, the key idea behind the diffuse-interface method is rather an old one. It has found extensive use in studies of critical phenomena such as phase separation (Hohenberg & Halperin 1977). Among those the most relevant to our work is perhaps Lapeña *et al.* (1999), who calculated different scenarios of phase separation when a mixture of flexible and rigid molecules is quenched below the critical point. Typically fluid flow is excluded from such studies. On the other hand, the diffuse-interface model has been developed as a tool for two-phase flows of Newtonian fluids (Anderson, McFadden & Wheeler 1998). For instance, Jacqmin (1999, 2000) simulated Rayleigh–Taylor instability, capillary waves and contact-line dynamics; Verschueren, van de Vosse & Meijer (2001) investigated thermocapillary flow instability in a Hele-Shaw cell; Badalassi, Ceniceros & Banerjee (2003) simulated phase separation under shear; and Liu & Shen (2003) studied bubble relaxation, rise and coalescence. Against this backdrop, the contribution of this paper is to put forth a formalism that systematically incorporates *complex fluid rheology* as well as interfacial dynamics. We view this work as the first step in developing the diffuse-interface idea into a unique CFD tool for multi-phase and multi-component complex fluids. The main objective here is to demonstrate the methodology and validate the numerical schemes by comparing with known results. Detailed exploration of new physics is deferred to a later study.

2. Theoretical and numerical models

The conservative dynamics of the diffuse-interface model can be formulated in the classical procedure of Lagrangian mechanics (Lowengrub & Truskinovsky 1998; Liu & Shen 2003). The starting point is the Lagrangian $L = T - F$, where T and F are the kinetic and potential energies of the system. The least-action principle requires that the action integral $I = \int L \, \mathrm{d}t$ be stationary under variations of 'paths'. This will lead to a momentum equation, with elastic stresses arising from the microstructural changes described by F, and evolution equations for the field variables whose momenta are included in T. The dissipative part of the dynamics is commonly derived via irreversible thermodynamics (de Groot & Mazur 1962). The entropy production is expressed as a sum of products of pairs of forces and fluxes, which are then made to be proportional to each other to yield the usual linear constitutive laws for viscous dissipation (Newtonian viscous stress), heat conduction (Fourier's law), mass diffusion (Fick's law), etc. Dissipations can also be accounted for through stochastic effects in the variational procedure (Peskin 1985; Gliklikh 1997).

It is the generality of this procedure, especially in accommodating microstructured fluids via the free energy F, that has made the diffuse-interface method our choice for tackling interfacial problems of complex fluids. Conceivably, any complex fluid with a properly defined free energy can be included in this formulation. In this paper, we will be dealing with two kinds: a viscoelastic fluid characterized by the Oldroyd-B model (Bird, Armstrong & Hassager 1987*a*), and a nematic liquid crystal described by a regularized Leslie–Ericksen model (Liu & Walkington 2000). The latter also introduces the issue of surface anchoring. In the following, we will derive the model equations for an immiscible blend of a nematic and a Newtonian fluid. Both are assumed to be incompressible and have the same density. The formulation for a blend of Oldroyd-B and Newtonian fluids is much simpler, and the key elements will be given before model validation in § 3.1. The issue of non-equal densities and non-solenoidal velocity will be briefly discussed at the end of § 2.4. Since the variational procedure for the least-action principle has been given before (Lowengrub & Truskinovsky 1998; Liu & Shen 2003), our focus will be on the non-Newtonian rheology.

2.1. *Free energies*

In an immiscible blend of a nematic liquid crystal and a Newtonian fluid, there are three types of free energy: mixing energy of the interface, bulk distortion energy of the nematic, and the anchoring energy of the liquid crystal molecules on the interface.

Mixing energy. In the diffuse-interface picture, the interface has a small but finite thickness, inside which the two components are mixed and store a mixing energy. We introduce a phase-field variable ϕ such that the concentration of the two components is $(1+\phi)/2$ and $(1-\phi)/2$, respectively. Following Cahn & Hilliard (1958), we express the mixing-energy density as a function of ϕ and its gradient:

$$f_{mix}(\phi, \nabla\phi) = \tfrac{1}{2}\lambda|\nabla\phi|^2 + f_0(\phi). \tag{1}$$

If we use a double-well potential for f_0

$$f_0 = \frac{\lambda}{4\epsilon^2}(\phi^2 - 1)^2, \tag{2}$$

then the physical meaning of equation (1) becomes apparent. The bulk energy f_0 prefers total separation of the phases into domains of the pure components ($\phi = \pm 1$). This 'phobic' effect produces the classical sharp-interface picture. The gradient term represents weakly non-local interactions between the components that prefers

complete mixing (a 'philic' effect). The profile of ϕ across the interface is determined by the competition between the two effects. λ is the magnitude of the mixing energy, while ϵ is a capillary width representative of the thickness of interface. Note the connection of equations (1), (2) to the Flory–Huggins–de Gennes mixing energy (de Gennes 1980).

Bulk distortion energy. The nematic has rod-like molecules whose orientation can be represented by a unit vector $\boldsymbol{n}(\boldsymbol{x})$ known as the director. When the director field is not uniform, the nematic has a Frank distortion energy (de Gennes & Prost 1993):

$$f_{bulk} = \tfrac{1}{2}K_1(\nabla\cdot\boldsymbol{n})^2 + \tfrac{1}{2}K_2(\boldsymbol{n}\cdot\nabla\times\boldsymbol{n})^2 + \tfrac{1}{2}K_3(\boldsymbol{n}\times\nabla\times\boldsymbol{n})^2, \tag{3}$$

where K_1, K_2, K_3 are elastic constants for the three canonical types of orientational distortion: splay, twist and bend. We will adopt the customary one-constant approximation: $K = K_1 = K_2 = K_3$, so that the Frank energy simplifies to $f_{bulk} = \frac{1}{2}K\nabla\boldsymbol{n} : (\nabla\boldsymbol{n})^{\mathrm{T}}$. A serious flaw of the Frank theory is its inability to describe defects, i.e. singular points in the $\boldsymbol{n}(\boldsymbol{x})$ field. Liu & Walkington (2000) circumvented this difficulty by allowing a non-unity director whose length indicates the order parameter. Thus, the regularized Frank elastic energy becomes

$$f_{bulk} = K\left[\tfrac{1}{2}\nabla\boldsymbol{n} : (\nabla\boldsymbol{n})^{\mathrm{T}} + \frac{(|\boldsymbol{n}|^2-1)^2}{4\delta^2}\right], \tag{4}$$

which will be used in our work. The second term on the right-hand side serves as a penalty whose minimization is simply the Ginzburg–Landau approximation of the constraint $|\boldsymbol{n}| = 1$ for small δ. The advantage of this regularized formulation is that the energy is now bounded for orientational defects, which are non-singular points where $|\boldsymbol{n}| = 0$. This makes the numerical treatment much easier. Note that the regularization is based on the same idea as in Cahn–Hilliard's mixing energy. It is also related to Ericksen's (1991) theory of uniaxial nematics with a variable order parameter.

Anchoring energy. Depending on the chemistry of the two components, the rod-like molecules of the nematic phase prefer to be oriented on the interface in a certain direction known as the easy direction. The anchoring energy is a measure of the penalty for deviating from the easy direction, which may occur as a result, for example, of flow, bulk distortion or an external field. The two most common types of anchoring are planar anchoring, where all directions in the plane of the interface are easy directions, and homeotropic anchoring, where the easy direction is the normal to the interface.

In the classical sharp-interface picture, the anchoring energy is a surface energy (Rapini & Popoular 1969). In our diffuse-interface model, however, we write it as a volumetric energy density in the same vein as the mixing energy:

$$f_{anch} = \tfrac{1}{2}A(\boldsymbol{n}\cdot\nabla\phi)^2 \tag{5}$$

for planar anchoring, and

$$f_{anch} = \tfrac{1}{2}A[|\boldsymbol{n}|^2|\nabla\phi|^2 - (\boldsymbol{n}\cdot\nabla\phi)^2] \tag{6}$$

for homeotropic anchoring. In these two equations, the positive parameter A indicates the strength of the anchoring.

Finally, the total free energy density for the two-phase material is written as

$$f(\phi, \boldsymbol{n}, \nabla\phi, \nabla\boldsymbol{n}) = f_{mix} + \tfrac{1}{2}(1+\phi)f_{bulk} + f_{anch} \tag{7}$$

where $\frac{1}{2}(1+\phi)$ is the volume fraction of the nematic component, and $\phi = 1$ in the purely nematic phase. This energy is equivalent to that of Rey (2000), and contains

all the physics discussed there, including a Marangoni force along isotropic–nematic interfaces.

2.2. *Interfacial tension and capillary width*

Since the mixing energy f_{mix} represents molecular interaction between the two phases, the classical concept of interfacial tension should be contained in it. We will derive a relationship between the parameters in equation (1) and an interfacial tension σ. This not only indicates the connection to the sharp-interface limit, but also gives us a rule for translating our parameters into the sharp-interface ones for comparison.

Consider a one-dimensional interface. We require that the diffuse mixing energy in the region be equal to the traditional surface energy:

$$\sigma = \lambda \int_{-\infty}^{+\infty} \left\{ \frac{1}{2} \left(\frac{\mathrm{d}\phi}{\mathrm{d}x} \right)^2 + f_0(\phi) \right\} \mathrm{d}x. \tag{8}$$

Let us further assume that the diffuse interface is at equilibrium, and thus has zero chemical potential,

$$\frac{\delta F_{mix}}{\delta \phi} = \lambda \left\{ -\frac{\mathrm{d}^2\phi}{\mathrm{d}x^2} + f_0'(\phi) \right\} = 0. \tag{9}$$

Since $f_0(\pm\infty) = 0$ and $\mathrm{d}\phi/\mathrm{d}x|_{x=\pm\infty} = 0$, this equation can be integrated once to give

$$\frac{1}{2} \left(\frac{\mathrm{d}\phi}{\mathrm{d}x} \right)^2 = f_0(\phi), \tag{10}$$

which implies equal partition of the free energy between the two terms at equilibrium.

Equation (10) can be solved together with the boundary condition $\phi(0) = 0$, and we obtain the equilibrium profile for $\phi(x)$:

$$\phi(x) = \tanh \left(\frac{x}{\sqrt{2}\epsilon} \right). \tag{11}$$

Thus, the capillary width ϵ is a measure of the thickness of the diffuse interface. More specifically, 90% of variation in ϕ occurs over a thickness of 4.1641ϵ, while 99% of the variation corresponds to a thickness of 7.4859ϵ. Note that the ϕ-profile in equation (11) gives the absolute minimum of the free energy, which also has many local minima corresponding to a family of periodic profiles (Mauri, Shinnar & Triantafyllou 1996).

Substituting equation (11) into equation (8), we arrive at the following matching condition for the interfacial tension σ:

$$\sigma = \frac{2\sqrt{2}}{3} \frac{\lambda}{\epsilon}. \tag{12}$$

Our derivation is similar to that of Jacqmin (1999), except that he starts from the stress rather than the energy. As the interfacial thickness ϵ shrinks toward zero, so should the energy density parameter λ; their ratio gives the interfacial tension in the sharp-interface limit. A formal proof of the diffuse-interface model converging to the conventional Navier–Stokes system with sharp interfaces can be found in, e.g., Liu & Shen (2003).

If the diffuse interface is not at equilibrium but is relaxing according to an evolution equation (cf. equation (23) below), one obviously cannot speak of a constant interfacial tension. Although this may seem to be a deficiency of the diffuse-interface model, it in fact reflects the reality that the interface has its own dynamics which cannot be

embodied by a constant σ except under limiting conditions. To anticipate the results in § 3.3, we note that f_{anch} may also contribute to the surface energy, thus giving rise to an anisotropic 'interfacial tension' that is not encompassed by the traditional version of the concept.

2.3. *Stress tensor*

Given the free energy of a system, an elastic stress tensor can be derived from the least-action principle. We will use a somewhat different version of the variational procedure, sometimes called the virtual work principle (Doi & Edwards 1986; Feng, Sgalari & Leal 2000), which operates on the potential energy only and is therefore more concise. For a volume Ω of our two-phase material, the total free energy is

$$F = \int_{\Omega} f(\phi, \boldsymbol{n}, \nabla\phi, \nabla\boldsymbol{n})\,\mathrm{d}\Omega. \tag{13}$$

Now we impose a virtual displacement $\delta\boldsymbol{x} = \boldsymbol{v}\delta t$ on the material in Ω, and consider the variation of F. In this process, ϕ and $\boldsymbol{n}$ are convected with the material point with no diffusion effect, i.e. $\delta\phi = 0$, $\delta\boldsymbol{n} = 0$. Noting that $\delta(\cdot) = (\partial(\cdot)/\partial t)\delta t + \delta\boldsymbol{x}\cdot\nabla(\cdot)$ is associated with the material derivative, we can derive the following identities:

$$\delta(\nabla\phi) = -\nabla(\delta\boldsymbol{x})\cdot\nabla\phi, \tag{14}$$

$$\delta(\nabla\boldsymbol{n}) = -\nabla(\delta\boldsymbol{x})\cdot\nabla\boldsymbol{n}. \tag{15}$$

Now the variation of F can be calculated:

$$\begin{aligned}
\delta F &= \int_{\Omega} \delta f\,\mathrm{d}\Omega \\
&= \int_{\Omega} \left[\frac{\partial f}{\partial\phi}\delta\phi + \frac{\partial f}{\partial\boldsymbol{n}}\cdot\delta\boldsymbol{n} + \frac{\partial f}{\partial\nabla\phi}\cdot\delta(\nabla\phi) + \frac{\partial f}{\partial\nabla\boldsymbol{n}} : \delta(\nabla\boldsymbol{n})^{\mathrm{T}}\right]\mathrm{d}\Omega \\
&= \int_{\Omega} \left[-\frac{\partial f}{\partial\nabla\phi}\otimes\nabla\phi - \frac{\partial f}{\partial\nabla\boldsymbol{n}}\cdot(\nabla\boldsymbol{n})^{\mathrm{T}}\right] : \nabla\delta\boldsymbol{x}^{\mathrm{T}}\,\mathrm{d}\Omega,
\end{aligned} \tag{16}$$

which, according to the virtual work principle, implies the following elastic stress tensor:

$$\boldsymbol{\sigma}^{e} = -\frac{\partial f}{\partial\nabla\phi}\otimes\nabla\phi - \frac{\partial f}{\partial\nabla\boldsymbol{n}}\cdot(\nabla\boldsymbol{n})^{\mathrm{T}}. \tag{17}$$

The above procedure uses $\nabla\cdot\delta\boldsymbol{x} = 0$ but does not explicitly subject the variation to the constraint of incompressibility: $J = |\partial\boldsymbol{x}/\partial\boldsymbol{X}| = 1$, $\boldsymbol{x}$ and $\boldsymbol{X}$ being the current and a previous configuration of the material. To be rigorous, therefore, we need to do the variation on a new functional $F' = F + \int_{\Omega}\lambda'(J-1)\,\mathrm{d}\boldsymbol{X}$, with a Lagrange multiplier $\lambda'(\boldsymbol{X})$. The extra term leads to an isotropic stress which can be absorbed into the pressure in the momentum equation. Thus, the elastic stress in equation (17) remains valid. Inserting equation (7) into equation (17), we arrive at the following elastic stress tensor:

$$\boldsymbol{\sigma}^{e} = -\lambda(\nabla\phi\otimes\nabla\phi) - K\tfrac{1}{2}(1+\phi)\,(\nabla\boldsymbol{n})\cdot(\nabla\boldsymbol{n})^{\mathrm{T}} - \boldsymbol{G}, \tag{18}$$

where $\boldsymbol{G} = A(\boldsymbol{n}\cdot\nabla\phi)\boldsymbol{n}\otimes\nabla\phi$ for planar anchoring and $\boldsymbol{G} = A[(\boldsymbol{n}\cdot\boldsymbol{n})\nabla\phi - (\boldsymbol{n}\cdot\nabla\phi)\boldsymbol{n}]\otimes\nabla\phi$ for homeotropic anchoring. Note that the asymmetry of $\boldsymbol{G}$ reflects the fact that surface anchoring exerts a net torque on the fluid. Bulk distortion will give rise to an asymmetric stress as well if the elastic constants are unequal (de Gennes & Prost 1993).

Aside from the elastic stress, there is also a viscous stress tensor. For a nematic liquid, the viscous stress is anisotropic in general and depends on the orientation of $\boldsymbol{n}$. For simplicity, we have used a Newtonian viscous stress in both components:

$$\boldsymbol{\sigma}^v = \mu[\nabla \boldsymbol{v} + (\nabla \boldsymbol{v}^T)]. \tag{19}$$

The viscosity μ may be different in the two phases. For numerical convenience, we have only computed equal-viscosity cases in this paper. As the main objective of this work is to demonstrate the methodology, the physical consequences of an anisotropic viscous stress will be explored in a later study. Finally, the total stress tensor $\boldsymbol{\sigma}$ is simply the sum of the elastic stress $\boldsymbol{\sigma}^e$ and the viscous stress $\boldsymbol{\sigma}^v$.

2.4. *Governing equations*

The general procedure for deriving the governing equations from the least-action principle has been outlined in Lowengrub & Truskinovsky (1998) and Liu & Shen (2003). In the following, therefore, we will simply list the equations for our particular case, with some remarks on the dissipative effects. For our model system of a blend of a nematic and a Newtonian fluid, the field variables are velocity $\boldsymbol{v}$, pressure p, phase function ϕ and director $\boldsymbol{n}$. We write the continuity and momentum equations in the usual form:

$$\nabla \cdot \boldsymbol{v} = 0, \tag{20}$$

$$\rho\left(\frac{\partial \boldsymbol{v}}{\partial t} + \boldsymbol{v} \cdot \nabla \boldsymbol{v}\right) = -\nabla p + \nabla \cdot \boldsymbol{\sigma}, \tag{21}$$

where $\boldsymbol{\sigma}$ is the deviatoric stress tensor. For complex fluids, fluid inertia is often negligible. Among the three problems to be simulated in § 3, we retain inertia only for the drop coalescence problem in § 3.2.

Cahn–Hilliard equation. Based on the free energy in equation (7), a generalized chemical potential can be defined as $\delta F/\delta\phi$. If one assumes a generalized Fick's law that the mass flux be proportional to the gradient of the chemical potential, the Cahn–Hilliard equation is obtained as an evolution equation for ϕ (Cahn & Hilliard 1959):

$$\frac{\partial \phi}{\partial t} + \boldsymbol{v} \cdot \nabla \phi = \nabla \cdot \left[\gamma_1 \nabla\left(\frac{\delta F}{\delta \phi}\right)\right] \tag{22}$$

where γ_1 is the mobility, taken to be a constant in this paper.

The diffusion term on the right-hand side has contributions from all three forms of free energy. In our calculations, we intend to approximate the sharp-interface limit, where the interface is driven entirely by advection. For simplicity, we neglect f_{bulk} and f_{anch} and retain only the mixing energy f_{mix} to produce the interface structure:

$$\frac{\partial \phi}{\partial t} + \boldsymbol{v} \cdot \nabla \phi = \gamma_1 \lambda \nabla^2 \left[-\nabla^2 \phi + \frac{\phi(\phi^2 - 1)}{\epsilon^2}\right]. \tag{23}$$

The parameter $\gamma_1 \lambda$ determines the relaxation time of the interface, and has to be chosen judiciously. Jacqmin (1999) has summarized the physical considerations that should go into choosing an interfacial relaxation time: "the straining flows can thin or thicken the interface and this must be resisted by a high enough diffusion. On the other hand, too large a diffusion will overly damp the flow."

In some of the problems discussed in § 3, periodic boundary conditions are used on the outer boundary. If the problem is aperiodic along a certain coordinate, as is the case for the shear flow simulations, we adopt the follow boundary conditions for the

relevant boundary segments (Jacqmin 1999):

$$\nabla\left(\frac{\delta F_{mix}}{\delta\phi}\right)\cdot\boldsymbol{m}=0, \tag{24}$$

$$\frac{\partial f_{mix}}{\partial(\nabla\phi)}\cdot\boldsymbol{m}=0, \tag{25}$$

where $\boldsymbol{m}$ is the normal of the boundary. The first is a no-flux condition as $\delta F_{mix}/\delta\phi$ is the generalized chemical potential. The second is a natural boundary condition required by the variational procedure. Using equations (1) and (2), the boundary conditions become simply

$$\frac{\partial\phi}{\partial m}=0, \tag{26}$$

$$\frac{\partial}{\partial m}(\nabla^2\phi)=0. \tag{27}$$

Director equation. The rotation of $\boldsymbol{n}$ is determined by the balance between a viscous torque and an elastic torque. The latter, also known as the molecular field (de Gennes & Prost 1993), arises from the free energies of the system:

$$\boldsymbol{h}=-\frac{\delta F}{\delta\boldsymbol{n}}=K\left[-\nabla\cdot\left(\tfrac{1}{2}(1+\phi)\nabla\boldsymbol{n}\right)+\tfrac{1}{2}(1+\phi)\frac{(\boldsymbol{n}^2-1)\boldsymbol{n}}{\delta^2}\right]+\boldsymbol{g}, \tag{28}$$

where $\boldsymbol{g}=A(\boldsymbol{n}\cdot\nabla\phi)\nabla\phi$ for planar anchoring, and $\boldsymbol{g}=A[(\nabla\phi\cdot\nabla\phi)\boldsymbol{n}-(\boldsymbol{n}\cdot\nabla\phi)\nabla\phi]$ for homeotropic anchoring. Now the evolution equation of $\boldsymbol{n}$ is written as

$$\frac{\partial\boldsymbol{n}}{\partial t}+\boldsymbol{v}\cdot\nabla\boldsymbol{n}=\gamma_2\boldsymbol{h}, \tag{29}$$

where the constant γ_2 determines the relaxation time of the director field.

Equations (18), (19) and (29) represent a simplified version of the Leslie–Ericksen theory (de Gennes & Prost 1993). Part of the viscous torque due to straining flow is omitted from equation (29), as are anisotropic viscous terms from the viscous stress tensor (equation (19)). The rationale for leaving out these dissipative terms is two-fold. First, the conservative dynamics dictates the trend in the system's evolution, while dissipation plays the secondary role of slowing down the process. Second, neglecting these terms brings about considerable savings in computation. If retained, they would couple the momentum equation closely with the director evolution, and entail iteration among the equations at every time step. If we omit these terms, the system can be solved semi-implicitly without iterations. Obviously, quantitatively accurate results require the full theory, which presents numerical complications but no conceptual difficulty (Lin & Liu 2000).

Equations (20), (21), (23) and (29) form the complete set of equations governing the evolution of the nematic–Newtonian two-phase system.

In this paper, we assume that the two phases have the same constant density, with negligible volume change upon mixing. Thus, the mixture is incompressible with a solenoidal velocity. In general, however, the diffuse-interface method is not restricted to equal-density components. When the two phases have differing densities, one approach is to view the mixture as a compressible fluid with $\nabla\cdot\boldsymbol{v}\neq 0$ in the mixing layer, where $\boldsymbol{v}$ is a mass-averaged velocity (Lowengrub & Truskinovsky 1998). As an alternative, Liu & Shen (2003) have proposed a picture in which the components mix by advection only without diffusion. Thus, the velocity at a spatial point is

defined as that of the component occupying that point; it is spatially continuous and remains solenoidal. An inhomogeneous average density is established from the initial condition, which is later transported by the velocity field. Finally, if the density difference is small, the Boussinesq approximation can be employed (Liu & Shen 2003).

2.5. *Energy conservation*

A solution to the above governing equations obeys an energy law. For example, multiplying equation (21) by the velocity $\boldsymbol{v}$, equation (22) by the chemical potential $\delta F/\delta\phi$ and equation (29) by the molecular field $\delta F/\delta \boldsymbol{n}$, integrating over the entire domain and summing the results, we obtain

$$\frac{\mathrm{d}}{\mathrm{d}t}\int_{\Omega}\left(\tfrac{1}{2}\rho|\boldsymbol{v}|^2+f\right)\mathrm{d}\Omega=-\int_{\Omega}\left(\mu\nabla\boldsymbol{v}:\nabla\boldsymbol{v}^{\mathrm{T}}+\gamma_1\left|\nabla\frac{\delta F}{\delta\phi}\right|^2+\gamma_2\left|\frac{\delta F}{\delta\boldsymbol{n}}\right|^2\right)\mathrm{d}\Omega, \qquad (30)$$

where f is the system's potential energy density (cf. equation (7)), and surface work has been omitted. Physically, the law states that the total energy of the system (excluding thermal energy) will decrease from internal dissipation. Based on such energy laws, Lin & Liu (1995, 2000) have established the existence of classical and weak solutions for Leslie–Ericksen fluids. In general, energy laws play an important role in the convergence of finite-dimensional approximations to partial differential equations, especially when the solution is not smooth (Liu & Walkington 2000). This constitutes one of the advantages of our method over previous methods that do not maintain the system's total energy budget.

For complex fluids, the energy estimate usually involves second-order derivatives of the microstructural conformation. This causes some difficulties for Galerkin finite elements, which Liu & Walkington (2000, 2002) have resolved by employing Hermite elements and later a more efficient mixed method. In this paper, we use the spectral method whose differentiable test functions avoid this complication. The trade-off is the limitation to relatively simple geometries and some special care in handling the boundary conditions.

2.6. *Numerical scheme*

In this paper, spectral methods are used to discretize the governing equations in two-dimensional rectangular domains. To enhance stability, we advance time semi-implicitly, with the nonlinear transport terms treated explicitly and the linear terms implicitly. Filters are sometimes employed to suppress spurious oscillations in the solution. To reduce the computational cost, the nonlinear terms are evaluated by Orszag's pseudospectral transform method (Canuto *et al.* 1987).

If periodic boundary conditions apply in both directions, we use the Fourier spectral method. A second-order backward difference formula (BDF) is used for the time derivatives and a second-order Adams–Bashforth (AB) scheme is used for the explicit treatment of nonlinear transport terms. Details of this second-order BDF/AB formulation can be found in Chen & Shen (1998). If we have periodic boundary conditions in one direction but aperiodic boundary conditions in the other, we use a Fourier spectral method along the former coordinate and a Chebyshev–Galerkin method along the latter, with a first-order BDF for the time derivatives. The base functions and direct solvers of the Chebyshev–Galerkin method have been described by Shen (1995) for Dirichlet and Neumann boundary conditions.

In the second case, aperiodicity calls for the boundary conditions in equations (26) and (27), the latter being neither Dirichlet nor Neumann. To impose them, we split the Cahn–Hilliard equation into two Helmholtz equations to which Neumann boundary

conditions apply as in Shen (1995). The time-discretized form of equation (23) is

$$\frac{\phi^{n+1}-\phi^n}{\Delta t}+(\boldsymbol{v}\cdot\nabla\phi)^n=\gamma_1\lambda\nabla^2\left[\left(-\nabla^2\phi+\frac{s\phi}{\epsilon^2}\right)^{n+1}+\left(\frac{(\phi^2-1-s)\phi}{\epsilon^2}\right)^n\right], \tag{31}$$

where the positive number s biases the scheme toward implicitness and enhances its stability. This equation can then be decomposed into two Helmholtz equations:

$$\left(\alpha+\frac{s}{\epsilon^2}\right)\psi-\nabla^2\psi=\frac{1}{\gamma_1\lambda}\left[-\frac{\phi}{\Delta t}+\boldsymbol{v}\cdot\nabla\phi-\gamma_1\lambda\nabla\left(\frac{(\phi^2-1-s)\phi}{\epsilon^2}\right)\right]^n, \tag{32}$$

$$(-\alpha\phi-\nabla^2\phi)^{n+1}=-\psi, \tag{33}$$

with boundary conditions $\partial\phi/\partial m=0$ and $\partial\psi/\partial m=0$, m being the normal to the boundary. The parameter

$$\alpha=-\frac{s}{2\epsilon^2}\left(1-\sqrt{1-\frac{4\epsilon^2}{\gamma_1\lambda s^2\Delta t}}\right),$$

such that ϕ^{n+1} cancels from equation (32) and ψ can be computed explicitly from ϕ^n. A real α requires $s\geqslant 2\epsilon^2/\sqrt{\gamma_1\lambda\Delta t}$, and we have used $s=\min(2\epsilon^2/\sqrt{\gamma_1\lambda\Delta t},2)$ in the calculations. If the fluid inertia is negligible, as is the case in § 3.1 and § 3.3, we advance all the dynamic equations in time, update the elastic stress and then calculate the velocity from the momentum (Stokes) equation.

Both the Fourier and Chebyshev methods utilize fast Fourier transform (FFT), which makes the computation very efficient. The computational complexity is quasi-optimal in the sense that the number of operations per time step is of $O(N\log N)$, N being the number of unknowns. On 750 MHz Sparc-v9 processors, the two-dimensional problems to be discussed in the next section typically take about 1 minute of CPU time every time step on a grid with adequate spatial resolution (1024×1024 or 2048×1024). Our meshing scheme is straightforward, with uniform mesh in a periodic direction and the Chebyshev–Gauss–Lobatto mesh in an aperiodic direction. The latter is convenient for implementing the Chebyshev discretization. As will be seen later, this simple meshing strategy is not optimal for resolving the interfaces, and a more sophisticated adaptive scheme is being developed.

For all the simulations reported in § 3, we have carried out grid and time-step refinements to ensure convergence. If we take 4.1641ϵ to be a nominal interfacial thickness (cf. equation (11)), this layer typically requires 7–10 grids to resolve. Coarser grids will generate spurious oscillations in the solution, especially in the vicinity of the interface. For the time step, we find the Courant–Friedricks–Lewy condition a useful guideline. In all cases tested, the temporal resolution is adequate as long as the simulation is stable.

An interesting numerical effect that is worth mentioning is the initial 'shift' of the ϕ-field. As an initial condition, we impose the hypertangential ϕ profile at the interface (equation (11)), with $\phi=\pm1$ in the two bulk phases. On commencing the simulation, however, we notice a very small shift in ϕ such that the interface $\phi=0$ shrinks slightly, and ϕ deviates from ±1 slightly in the bulk. Physically, the interface tends to shrink to reduce the mixing energy. Since $\int_\Omega\phi\,\mathrm{d}\Omega$ is conserved by the Cahn–Hilliard equation with the zero-flux boundary condition (equation (26)), the shrinking interface causes the bulk ϕ value to change, incurring a bulk energy penalty through the energy f_0 (equation (2)). The competition between the two effects results in a slightly relaxed ϕ-field that has a lower energy than our initial condition. For a circular drop of

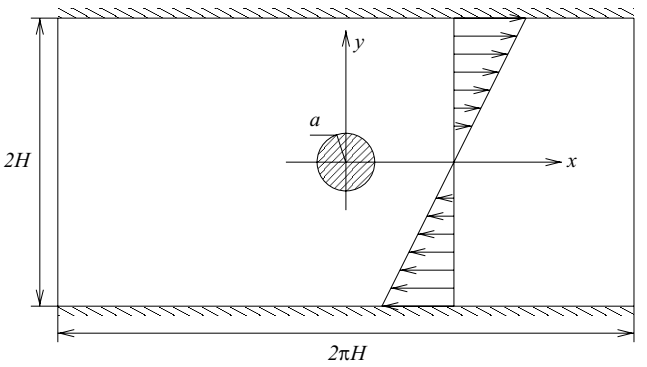

FIGURE 1. Schematic of the computational domain for a drop deforming in shear flow.

radius r, the shift in the bulk value of ϕ can be calculated: $\mathrm{d}\phi = \sqrt{2}\epsilon/6r$. We choose our ϵ so that $\mathrm{d}\phi$ is around 0.5%. Although this effect is insignificant in terms of the accuracy of the results, it nicely illustrates the relationship between interfacial and bulk properties that is at the heart of the diffuse-interface formulation.

3. Numerical results

This section has two objectives. First, by solving problems with previously published solutions, we seek to validate our theoretical and numerical schemes by comparison. Second, we will apply the diffuse-interface model to previously unsolved problems, and give some indications on the capability of our toolkit for interfacial flows of complex fluids. Comprehensive exploration of new physics will be carried out in future work.

We will report simulations on three problems: drop deformation in shear flows, head-on collision between two drops, and retraction of a nematic drop in a quiescent matrix. The first two problems are mainly intended to serve the first purpose, while the last problem addresses interesting questions raised by recent experiments on measuring interfacial tension between a liquid-crystalline polymer and a flexible polymer.

3.1. *Drop deformation in shear flows*

Flow-induced drop deformation is a well-researched problem. Earlier studies dealt with the situation where both the drop and the matrix phases are Newtonian viscous fluids. Rallison (1984) reviewed asymptotic solutions, boundary integral calculations and experiments. Stone (1994) surveyed newer results on drop breakup and the effects of surfactants. More recently, two- and three-dimensional numerical solutions have been obtained using boundary-integral (Zhou & Pozrikidis 1993; Cristini *et al.* 1998), boundary-element (Toose *et al.* 1995; Hooper *et al.* 2001*a*), finite-element (Kim & Han 2001; Ambravaneswaran *et al.* 2002), finite-difference (Ramaswamy & Leal 1999*a*), VOF (Li & Renardy 2000*a*) and level-set methods (Pillapakkam & Singh 2001), for Newtonian and viscoelastic liquids. Since our code is limited to two dimensions at present, we have chosen as benchmarks Zhou & Pozrikidis' (1993) boundary-integral calculation of a Newtonian–Newtonian system and Pillapakkam & Singh's (2001) level-set simulation of a Newtonian drop in an Oldroyd-B matrix.

Newtonian drop deforming in a Newtonian matrix. A schematic of the computational domain is shown in figure 1. The geometric setup is the same as in Zhou & Pozrikidis (1993), with a $[2\pi H \times 2H]$ computational domain. The drop sits at the centre; it

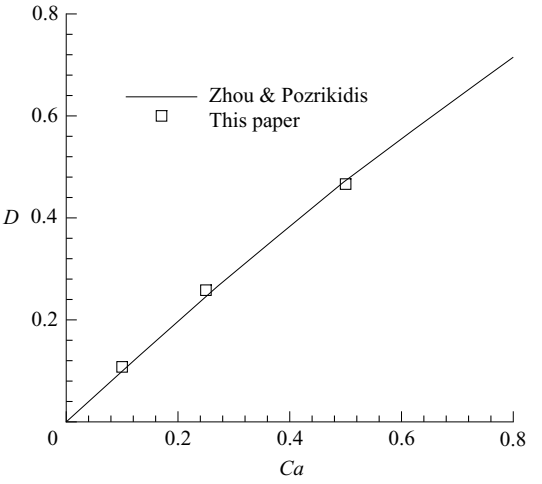

FIGURE 2. Comparison of the steady-state deformation of a Newtonian drop in a Newtonian matrix between our results and those in Zhou & Pozrikidis (1993).

is initially circular with a radius $a = H/4$. The shear rate is κ, and the drop and matrix phases have the same viscosity μ. Fluid inertia is neglected. We use H as the characteristic length and the inverse shear rate $1/\kappa$ as the characteristic time. In dimensionless terms, we have chosen a capillary width $\epsilon = 0.01$ and a mobility $\gamma_1 = 10^{-4}$. The interfacial tension σ is determined from equation (12); λ is varied to achieve different values of the capillary number defined by

$$Ca = \frac{\mu a \kappa}{\sigma}. \tag{34}$$

Note that Zhou & Pozrikidis' definition of Ca differs from ours by a factor of 4, and we have converted theirs in making the comparison. We have done numerical experiments to ensure that a time step $\Delta t = 1 \times 10^{-3}$ and grid numbers 2048×1024 offer adequate temporal and spatial resolution. In terms of the drop deformation, doubling or halving Δt brings about less than 0.2% of relative change. Halving the grid number in each direction causes less than 0.09% of change.

Figure 2 illustrates the steady-state deformation of the drop for several capillary numbers, in terms of a deformation parameter D defined as $D = (L - B)/(L + B)$, L and B being the drop's half-length and half-width, respectively. The agreement between the sharp-interface and diffuse-interface results is excellent; the maximum difference in the steady-state value of D is within 4%. The history of deformation $D(t)$ is also in good agreement between the two studies.

Viscoelastic drop deforming in a Newtonian matrix. Pillapakkam & Singh (2001) used the level-set method to calculate the deformation of a two-dimensional Newtonian drop in a simple shear of an Oldroyd-B fluid. To incorporate the Oldroyd-B rheology into our scheme, we consider the viscoelastic fluid as a dilute suspension of polymer molecules, each represented by a Hookean dumbbell (Bird *et al.* 1987*b*). Given the configuration distribution function $\Psi(\boldsymbol{Q}, \boldsymbol{x}, t)$, where $\boldsymbol{Q}$ is the connector vector of the dumbbell, the free energy of a single molecule can be written as

$$f_p(\Psi) = kT\Psi \ln(\Psi) + \tfrac{1}{2} K_H (\boldsymbol{Q} \cdot \boldsymbol{Q}), \tag{35}$$

where k is the Boltzmann constant, T is the temperature and K_H is the spring constant

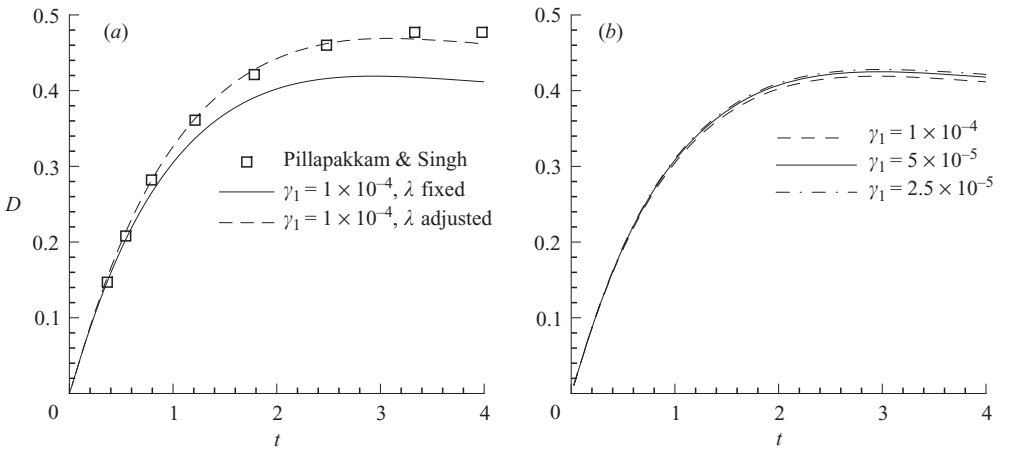

FIGURE 3. Transient deformation of a Newtonian drop in an Oldroyd-B fluid undergoing shear flow. $Ca = 0.24$, $De = 0.4$, $\epsilon = 0.01$. (*a*) Comparison with the result of Pillapakkam & Singh (2001): the significance of instantaneous matching of the interfacial tension. (*b*) Effects of the interfacial mobility γ_1 for a fixed λ.

of the Hookean dumbbell. Then the extra free energy due to the dumbbells in the Oldroyd-B/Newtonian two-phase system is

$$F = \int_{\Omega} \left[\tfrac{1}{2}(1+\phi) n \int_{R^3} f_p \, \mathrm{d}\boldsymbol{Q} \right] \mathrm{d}\Omega, \tag{36}$$

where n is the number density of dumbbells in the Oldroyd-B fluid, and $\phi = 1$ for the Oldroyd-B matrix phase.

Incorporating this extra free energy into the variation procedure outlined in the last section, we readily derive an extra stress tensor for the Oldroyd-B/Newtonian two-phase system:

$$\boldsymbol{\sigma}_p = \tfrac{1}{2}(1+\phi) n(-kT\boldsymbol{I} + K_H \langle \boldsymbol{Q}\boldsymbol{Q} \rangle) = \tfrac{1}{2}(1+\phi)\boldsymbol{\tau}_p, \tag{37}$$

where $\langle \cdot \rangle = \int_{R^3} \cdot \, \Psi \, \mathrm{d}\boldsymbol{Q}$, and $\boldsymbol{I}$ is the identity tensor. The polymer stress $\boldsymbol{\tau}_p$ is identical to that derived in kinetic theory (Bird *et al.* 1987*b*), and it obeys the upper-convected Maxwell equation

$$\boldsymbol{\tau}_p + \lambda_H \boldsymbol{\tau}_{p(1)} = \mu_p \left[\nabla \boldsymbol{v} + (\nabla \boldsymbol{v})^{\mathrm{T}} \right], \tag{38}$$

in which the subscript (1) denotes the upper convected derivative

$$\boldsymbol{A}_{(1)} = \frac{\partial \boldsymbol{A}}{\partial t} + \boldsymbol{v} \cdot \nabla \boldsymbol{A} - (\nabla \boldsymbol{v})^{\mathrm{T}} \cdot \boldsymbol{A} - \boldsymbol{A} \cdot \nabla \boldsymbol{v},$$

λ_H is the time constant for Hookean dumbbells, and μ_p is a polymer viscosity.

With the stress tensor properly formulated, the other governing equations – the Cahn–Hilliard equation, the continuity and momentum equations – are the same as the Newtonian–Newtonian case. The parameters in Pillapakkam & Singh (2001) are: $Ca = 0.24$, $De = 0.4$, $Re = 0.0003$, $a/H = 0.2$, $\mu_p = \mu_s = \mu_d$, where $De = \lambda_H \kappa$ is the Deborah number, and μ_p, μ_s and μ_d are the polymer and solvent viscosity in the matrix and the Newtonian drop viscosity. We use the same parameters except that $Re = 0$. In the following, time is scaled by $1/\kappa$.

Figure 3(*a*) compares our results with that of Pillapakkam & Singh (2001). The solid curve uses a fixed λ value determined by equation (12) to match the surface tension.

The drop deformation is about 13% below that of Pillapakkam & Singh (2001). This turns out to be a consequence of *interfacial relaxation*. Recall that equation (12) is derived for the equilibrium ϕ profile across a one-dimensional interface, which may not be the equilibrium ϕ for a circular drop. Furthermore, as the drop deforms, the interfacial ϕ profile is disturbed as well. In this case, the deviation from the hyperbolic tangent ϕ in equation (11) amounts to an overall increase in the mixing energy per unit interfacial length. Thus, with a fixed λ, the 'effective interfacial tension' of our diffuse interface increases with drop deformation, thereby inhibiting the latter. To minimize this effect, one should reduce the interfacial thickness and therefore suppress the role of interfacial relaxation. With our simple meshing scheme (cf. § 2.6), however, this would entail a great increase of grid numbers and computational cost. As an alternative, we have experimented with a correction scheme that adjusts the λ value at each time step so the total mixing energy at that moment matches the target surface tension:

$$\sigma S = \int_{\Omega} \lambda \left\{ \frac{|\nabla \phi|^2}{2} + \frac{1}{4\epsilon^2}(\phi^2 - 1)^2 \right\} \mathrm{d}\Omega, \tag{39}$$

where S is the circumference of the interface, and can be evaluated by integration along the contour of $\phi = 0$. The correction brings the maximum difference from the result of Pillapakkam & Singh (2001) from 13% down to 3% in figure 3(*a*). This confirms our conjecture that interfacial relaxation causes an elevated 'effective interfacial tension' and suppresses drop deformation. Another manifestation of interfacial relaxation is that after attaining maximum deformation, D decreases slightly, causing the curve to sag toward the end. This is due to a relaxation of the drop shape toward a circle that accompanies the relaxation of the interfacial ϕ-profile. We have also examined the role of interfacial relaxation in the Newtonian case (figure 2). Adjusting λ according to equation (39) leads to a mere 4% change in the steady-state D. The reason for the weaker effect is that the capillary width ϵ is smaller relative to the drop size in that case.

A related issue is the effect of the interfacial mobility parameter γ_1 (cf. equation (22)). With decreasing γ_1, interfacial relaxation becomes slower. The flow will thin or thicken the interface at different locations, driving it far from equilibrium. This exacerbates the uncertainty in matching the surface tension. But slower interfacial relaxation also delays the sagging of the D-curves. The overall effect of decreasing γ_1 is a slight increase in drop deformation (figure 3*b*). For large values of γ_1, on the other hand, interfacial diffusion is fast and the interface is almost always near its equilibrium state. The trade-off is that the dissipation will damp the flow near the interface (Jacqmin 1999). This may affect the quality of the solution, especially near critical events such as interface rupture and reconnection. Note also that there are situations where the interfacial relaxation itself is of interest (Warren & Boettinger 1995). Then γ_1 should be chosen by the corresponding physical criterion.

When simulating large-scale problems with complex interfaces, the correction scheme of equation (39) will be impractical, and one has to resolve the interface well with a large number of grid points inside a narrow region. This is a fundamental challenge with the phase-field representation (Sethian & Smereka 2003). Recently, Biben *et al.* (2003) presented an interesting alternative for suppressing the effects of interfacial relaxation. By removing the curvature-driven diffusion from the phase-field equation and adding the interfacial tension to the momentum equation as a smoothed δ-function, this advected-field approach integrates the level-set and

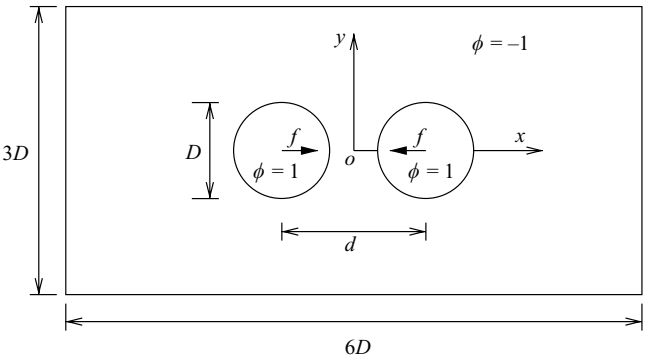

FIGURE 4. Computational domain for head-on collision between Newtonian drops. The initial separation is $d = 1.5D$.

phase-field ideas. In our context, however, this would undo the advantages of the energy-based formalism.

3.2. *Head-on collision between two drops*

We use the head-on collision and coalescence of two identical Newtonian drops in a Newtonian medium to demonstrate the ability of our method to handle singular topological changes. Nobari, Jan & Tryggvason (1996) solved a similar problem using the front-tracking method, where coalescence is effected by artificially rupturing the film at a prescribed time. We use a two-dimensional rectangular computational domain shown in figure 4, with periodic boundary conditions in both directions. Initially, two stationary drops of diameter D are separated by a centre-to-centre distance d. Then a body force $\boldsymbol{f}$ is applied to move the drops toward each other. When the drop velocity attains a prescribed value $U/2$, $\boldsymbol{f}$ is turned off. Carried on by inertia, the two drops collide and coalesce. The setup of the problem mimics that of Nobari *et al.* (1996), except that their geometry is axisymmetric while ours is two-dimensional. We further assume that the drop and matrix phase have the same viscosity and density so as to simplify the solution procedure. These differences preclude quantitative comparison with Nobari *et al.* (1996), but the simulation still affords us an opportunity to test the capability of the diffuse-interface method for simulating film drainage and rupture.

The dimensionless momentum equation is written as

$$\frac{\partial \boldsymbol{v}}{\partial t} + \boldsymbol{v}\cdot\nabla\boldsymbol{v} = -\nabla p + \frac{1}{Re}\nabla^2\boldsymbol{v} - \frac{3\epsilon}{2\sqrt{2}}\frac{1}{We}\nabla\cdot(\nabla\phi\otimes\nabla\phi) + \boldsymbol{f}, \tag{40}$$

where the characteristic length is D, the characteristic velocity U is the relative velocity between the drops when the body force $\boldsymbol{f}$ is turned off, and the characteristic time is D/U. Re and We are the Reynolds and Weber numbers, respectively. The coefficient before the interface stress term comes from matching our parameters λ and ϵ to the classic interfacial tension σ by equation (12).

Figure 5 shows the collision and coalescence of two drops for the following parameters: $Re = 33.6$, $We = 12$, $\epsilon = 0.01$ and the Cahn–Hilliard mobility $\gamma_1 = 3.365 \times 10^{-5}$. The body force $\boldsymbol{f} = (-4.44\mathrm{sign}(x)\frac{1}{2}(1+\phi), 0)$ is turned on at $t = 0$ and off at $t = 0.336$. The simulation was carried out on a 2048×1024 grid with time step $\Delta t = 3.365 \times 10^{-4}$; we have tested different time steps and mesh sizes to ensure adequate resolution. As in Yang *et al.* (2001), we can divide the process into three stages: drop transport

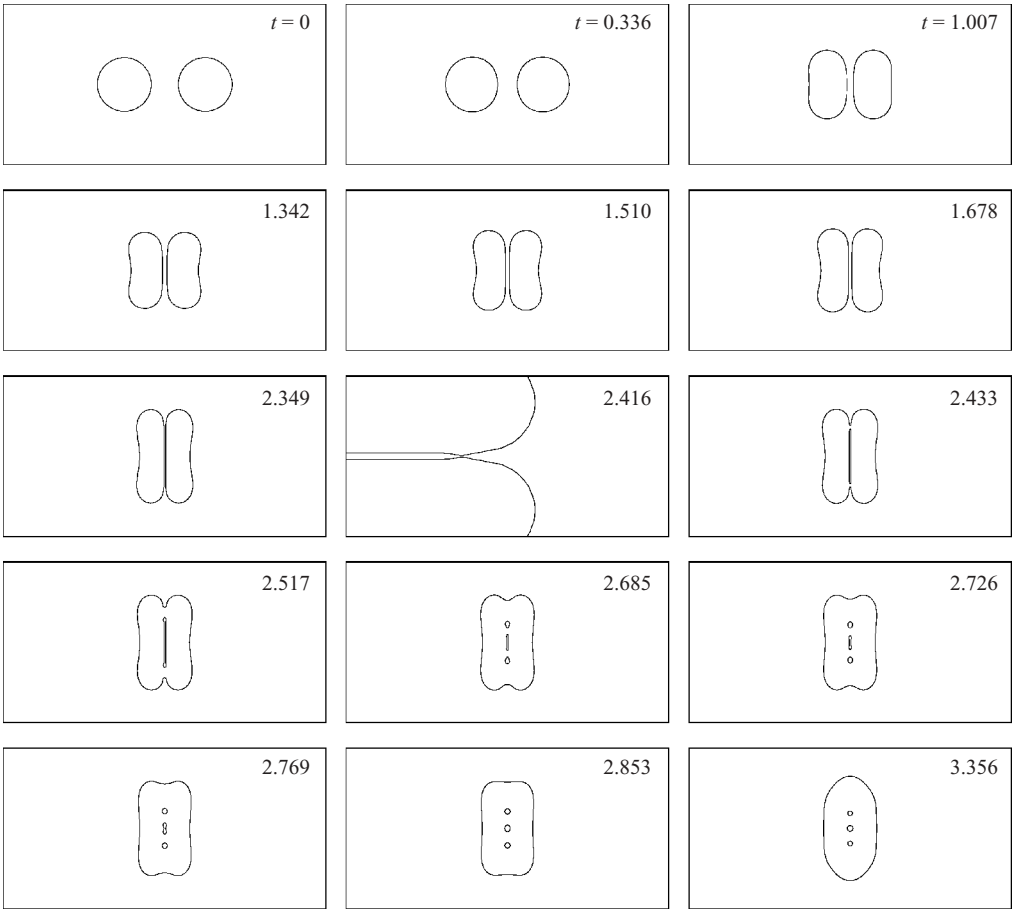

FIGURE 5. Collision and coalescence of two drops. $Re = 33.6$, $We = 12$. The magnified and rotated view at $t = 2.416$ shows the dimpled interface prior to film rupture.

($0 < t < 1.342$), film drainage ($1.342 < t < 2.416$) and coalescence ($t > 2.416$). A notable feature is the well-known dimpled shape of the interface before film rupture at $t = 2.416$. After film rupture, a filament of the matrix fluid is trapped inside the coalescing drops. These features qualitatively agree with prior experimental and theoretical results (Chuang & Flumerfelt 1997; Yang *et al.* 2001). The subsequent breakup of the filament ($2.517 < t < 2.769$) resembles the 'end-pinching' scenario described by Stone & Leal (1989), but cannot be a capillary effect since this is in two dimensions. Numerical experiments show that it is caused by the stretching flow due to the expansion of the waist of the compound drop. The general shape of the drops during collision is similar to the result of Nobari *et al.* (1996). Since their drops are much denser than the matrix and carry more momentum, the drop deformation is more severe than in our case. But the main difference between the two studies is the treatment of coalescence. By removing the film separating the drops artificially, Nobari *et al.* (1996) do not trap the matrix fluid. The subsequent dynamics of the new drop depends to some extent on the timing of the artificial rupture. Our method eliminates the need for such a device. The breakage and reconnection of the interfaces occur naturally from the Cahn–Hilliard dynamics (cf. equation (23)). In reality, the rupture of the interface is a result of the attractive van der Waals forces between the molecules

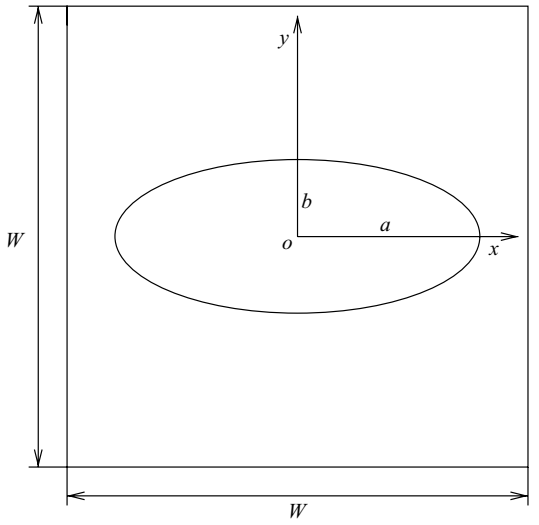

FIGURE 6. Computational domain for drop retraction. $W = 2\pi b$, $a = 2.5b$.

of the two drops. This type of molecular interaction is what the Cahn–Hilliard mixing energy represents. Thus, the coalescence simulated using the diffuse-interface model has captured, to some extent, the true physics of the process.

3.3. *Retraction of a nematic drop in a quiescent medium*

Drop retraction is a popular method for measuring the interfacial tension between the drop and matrix fluids (Mo, Zhou & Yu 2000; Son & Yoon 2001). The basis of this measurement is the relationship between the evolution of the drop shape and the interfacial tension. Various formulae have been developed by assuming Newtonian rheology in both the drop and the matrix phases. For instance, a phenomenological model due to Maffettone & Minale (1998) describes the retraction of an ellipsoidal drop by

$$L^2 - B^2 = (L^2 - B^2)_{t=0} \exp\left[-\frac{\sigma}{\mu_m R_0} \frac{40(\beta+1)}{(2\beta+3)(19\beta+16)} t\right], \tag{41}$$

where R_0 is the equilibrium drop radius, μ_m is the matrix viscosity and β is the viscosity ratio between the drop and the matrix. By measuring $L(t)$ and $B(t)$, the half-length and half-width of the drop, σ can be calculated from curve fitting. For some two-phase systems, equation (41) has been shown to give fairly good results (Mo *et al.* 2000). For a thermotropic liquid crystalline polymer (TLCP) drop retracting in a flexible polymer matrix, however, Yu *et al.* (2004) found that the drop size deviates from the exponential law. If equation (41) is applied to fit the slope of $\ln(L^2 - B^2)$ versus time at each data point, an apparent interfacial tension is obtained which declines with time. This seems to contradict the idea that the interfacial tension is a material constant.

Our aim in this sub-section is to investigate this phenomenon by numerical simulations, and present some preliminary insights revealed by the numerical results. Although the calculations are in two dimensions, we expect these physical insights to be relevant to the three-dimensional experiments. As in previous theoretical and numerical calculations, we assume the retraction is slow and the fluids are highly viscous so as to render inertia negligible.

The computational domain is shown in figure 6. We use periodic boundary condition for both directions and discretize the equations using a Fourier spectral method. Three

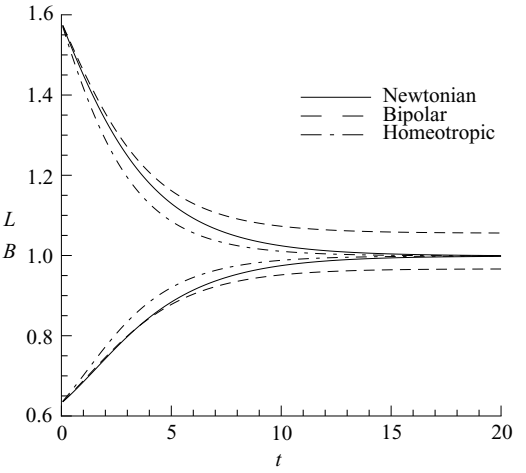

FIGURE 7. Retraction of a Newtonian drop and nematic drops with planar and homeotropic anchoring: variation of the semi-axes during retraction.

cases have been simulated, with the drop being Newtonian (baseline case), nematic with planar anchoring and nematic with homeotropic anchoring. The matrix fluid is always Newtonian, and the viscosity ratio is taken to be unity for simplicity. Initially, the drop is elliptic with semi-axes $a = 2.5b$ and $b = W/(2\pi)$. We will use the final drop radius R_0 as the characteristic length. Then in dimensionless terms, $W = 3.974$ and initially $a = 1.581$, $b = 0.6325$. If we use the capillary time scale $\mu_m R_0/\sigma$, the other dimensionless parameters have the following values: $\lambda = 1.342 \times 10^{-2}$, $\gamma_1 = 4 \times 10^{-5}$, $\epsilon = 1.265 \times 10^{-2}$, $\delta = 6.325 \times 10^{-2}$, $K = 6.708 \times 10^{-2}$, $A = 6.708 \times 10^{-3}$ and $\gamma_2 = 10$. Compared with the material constants of common liquid crystals and liquid crystal polymers (Larson 1999), the anchoring energy A is in the realistic range, while the bulk elastic constant K and director relaxation parameter γ_2 are about an order of magnitude too large. These are used to amplify the novel effects induced by the liquid crystallinity inside the drop. For planar anchoring, $\boldsymbol{n}$ is initially horizontal everywhere. For homeotropic anchoring, we impose a radial $\boldsymbol{n}$ emanating from the centre of the drop. Since the drop is elliptic, the initial $\boldsymbol{n}$-field deviates from the easy direction over much of the interface in both cases.

Figure 7 shows that the retraction occurs at different speeds for the three cases. The nematic drop with homeotropic anchoring retracts fastest while that with planar anchoring retracts slowest. This can be easily understood in terms of the anchoring energy. Given the initial $\boldsymbol{n}$-fields, the retraction reduces the anchoring energy for homeotropic anchoring but increases it for planar anchoring. In addition, the final equilibrium shape is circular for the Newtonian drop and the nematic drop with homeotropic anchoring, but is prolate for the nematic drop with planar anchoring. To understand this difference, we plot the equilibrium director fields inside the drops in figure 8. With homeotropic anchoring, a purely radial $\boldsymbol{n}$-field coupled with a circular shape minimizes the mixing energy f_{mix} and anchoring energy f_{anch}, at the expense of the bulk distortion energy f_{bulk}. A defect of strength $+1$ resides at the centre of the drop. With planar anchoring, on the other hand, there is a direct competition between f_{mix} and $f_{anch} + f_{bulk}$. The former favours a circular shape while the latter tends to elongate the drop so as to respect the tangential easy direction on the interface. The equilibrium shape results from a compromise between them.

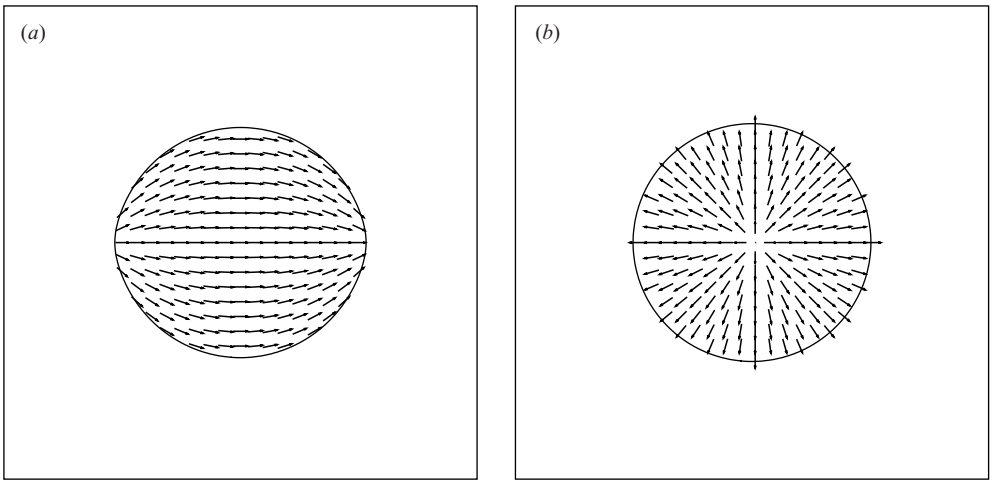

FIGURE 8. Director field inside the nematic drop at equilibrium. (*a*) A bipolar configuration with planar anchoring; (*b*) a radial configuration with homeotropic anchoring. For clarity, the director is plotted every 8 grid points in each direction.

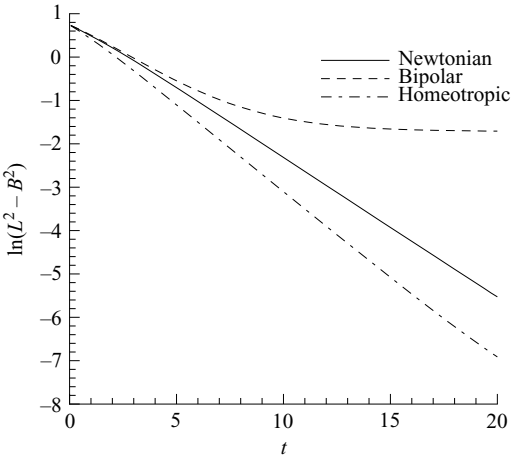

FIGURE 9. Retraction of a Newtonian drop and nematic drops with planar and homeotropic anchoring: $\ln(L^2 - B^2) \sim t$ curves used for fitting the Maffettone–Minale formula.

The *bipolar* configuration in figure 8(*a*), with two surface defects at the poles, is well-known in the liquid crystal literature (West 1990). The prolate equilibrium shape has been observed in the simulations of Lapeña *et al.* (1999) and the calculations of Huang & Tuthill (1994) and Calderer & Shen (2002). We have tested weaker K values representative of real materials; the prolateness of the bipolar drop is much reduced.

Figure 9 plots the $\ln(L^2 - B^2) \sim t$ curves for the three drops. According to the Maffettone–Minale model, the Newtonian drop should follow a straight line, which is indeed the case in our simulation except for the initial moments of the retraction. This is interesting since equation (41) is derived for a three-dimensional drop while ours is two-dimensional. The homeotropic drop follows a straight line as well, but with a steeper slope than the Newtonian drop. The drop with planar anchoring starts

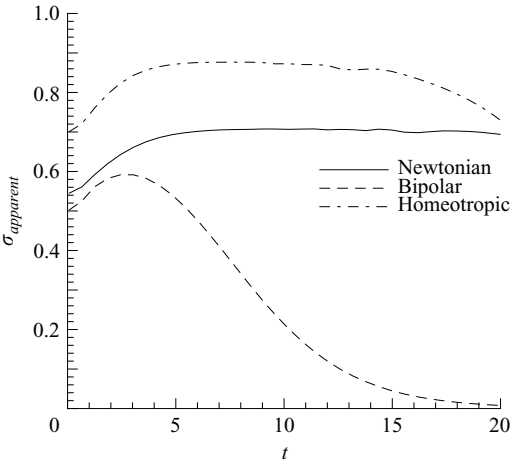

FIGURE 10. Temporal evolution of the apparent interfacial tension calculated from the slope of the curves in figure 9 using the Maffettone–Minale formula.

with a milder slope, and levels off toward the end of the retraction as it fails to attain a circular shape. If we still use the Maffettone–Minale model to calculate an apparent interfacial tension σ_a from the slope of the curves, it will vary in time as shown in figure 10.

In all three cases, σ_a rises at the beginning as the initially imposed hypertangential ϕ-profile relaxes. After the initial transient, σ_a remains essentially constant for the Newtonian drop. Our scaling is such that if the Maffettone–Minale model applies perfectly, σ_a should be unity. The lower value in figure 10 for the Newtonian drop reflects the fact that a drop retracts more slowly in two than in three dimensions. The nematic drop with homeotropic anchoring exhibits a large σ_a thanks to f_{anch}, which in this case favours a circular drop and assists the retraction. For the nematic drop with planar anchoring, however, σ_a experiences a rapid decline that is reminiscent of the experiment of Yu *et al.* (2004). To explore its origin, we use the stress field to calculate the surface force along the interface, which allows us to define a 'true interfacial tension' using the local curvature of the interface. This true interfacial tension exhibits a remarkable anisotropy, i.e. disparity between the poles and the equator of the drop. It is mainly the mounting penalty in the anchoring energy f_{anch} at the poles that resists retraction of the drop and gives rise to the sharp decline in σ_a. This is visually intuitive; it is at the poles that the retraction causes the most conflict between surface anchoring and bulk orientation, producing the surface defects. Compared with the Newtonian curve, f_{anch} is responsible for the generally lower value of σ_a and its asymptote toward zero as the drop approaches a non-circular final shape. The role of f_{anch} in the dynamic interfacial tension as revealed here is consistent with Rey's (2000) theory on sharp nematic interfaces.

The declining σ_a in figure 10 bears a clear similarity to the experimental results of Yu *et al.* (2004), and one is tempted to attribute this to an energy f_{anch} for planar anchoring. Polarized microscopy does indicate planar anchoring on the surface of a TLCP drop in a flexible polymer matrix (Wu & Mather 2002). One caveat has to be mentioned, however. The experimental drops are tens of microns in size, and contain a multitude of domains (Wu & Mather 2002). Inside each domain, $\boldsymbol{n}$ may be more or less uniform. But among the domains, the preferred orientation may

be rather random. This explains why experimentally the TLCP drops always retract to spheres instead of prolate spheroids. Nevertheless, the fundamental mechanism uncovered by the simulations, namely the planar anchoring producing a declining apparent interfacial tension, should have played a major role in the experiments.

4. Concluding remarks

In this paper, we derive a diffuse-interface formulation for computing interfacial flows of complex fluids such as the Oldroyd-B fluid and nematic liquid crystals. The formulation is applied to several problems to demonstrate its accuracy and efficiency, its potential in exploring complex physics, as well as its limitations. Besides its capability in handling large interfacial morphological changes, the method enjoys two unique advantages: the ease with which a wide range of complex rheology can be accommodated, and the conservation of energy which guarantees numerical convergence. Both stem from the underlying variational framework.

The rationale of using a diffuse-interface model instead of the classical sharp-interface model can be viewed from two different angles. The former can be seen as a numerical regularization of the latter, with the purpose of approximating the sharp-interface limit. Conversely, we may think of the diffuse interface as representing physical reality, and regard the sharp interface as a mathematical abstraction analogous to the concept of a shock wave. Such arguments are more than mere philosophical exercises; they bear directly on the choice of parameters and the interpretation of results. For instance, figure 3(*a*) reveals the subtlety in matching the diffuse-interface parameters to the conventional surface tension. On the one hand, we recognize that making the interface thinner reduces the degree of uncertainty. On the other hand, we may also view the surface tension as a convenient replacement for the more complex interfacial dynamics that occur in reality. The same dichotomy applies when comparing sharp-interface and diffuse-interface results.

We have also highlighted the special challenges in diffuse-interface models, the foremost being the need to resolve the interface adequately. The interfacial thickness in the simulations presented here is typically much larger than realistic values. This results from our need to resolve the interface while keeping the computational cost manageable. As a tradeoff, we have to deal with numerical issues such as the 'shift of ϕ' and the choice of the interfacial relaxation parameters (Jacqmin 1999). In ongoing work, we are developing an adaptive meshing strategy that aims to enhance the resolution of the interface and essentially eliminates the artificial numerical effects. Thus, on the whole, we conclude that the diffuse-interface model can be a powerful tool for simulating multiphase flows of complex fluids.

Acknowledgment is made to the Donors of The Petroleum Research Fund, administered by the American Chemical Society, for partial support of this research. J. J. F. was also supported by NSERC's Canada Research Chair program and by the NSF via grants CTS-0229298 and CTS-9984402. J. S. was supported by the NSF via grants DMS-0074283 and DMS-0311915. We acknowledge discussions with Professor Sanjoy Banerjee, Professor George (Bud) Homsy and Professor Jorge Viñals.

REFERENCES

Ambravaneswaran, B., Wilkes, E. D. & Basaran, O. A. 2002 Drop formation from a capillary tube: Comparison of one-dimensional and two-dimensional analyses and occurrence of satellite drops. *Phys. Fluids* **14**, 2606–2621.

Anderson, D. M., McFadden, G. B. & Wheeler, A. A. 1998 Diffuse-interface methods in fluid mechanics. *Annu. Rev. Fluid Mech.* **30**, 139–165.

Badalassi, V. E., Ceniceros, H. D. & Banerjee, S. 2003 Computation of multiphase systems with phase field model. *J. Comput. Phys.* **190**, 371–397.

Biben, T., Misbah, C., Leyrat, A. & Verdier, C. 2003 An advected-field approach to the dynamics of fluid interfaces. *Europhys. Lett.* **63**, 623–629.

Bird, R. B., Armstrong, R. C. & Hassager, O. 1987*a* *Dynamics of Polymeric Liquids, Vol. 1. Fluid Mechanics*. Wiley.

Bird, R. B., Curtiss, D. F., Armstrong, R. C. & Hassager, O. 1987*b* *Dynamics of Polymeric Liquids, Vol. 2. Kinetic Theory*. Wiley.

Cahn, J. W. & Hilliard, J. E. 1958 Free energy of a nonuniform system. I. Interfacial free energy. *J. Chem. Phys.* **28**, 258–267.

Cahn, J. W. & Hilliard, J. E. 1959 Free energy of a nonuniform system. III. Nucleation in a two-component incompressible fluid. *J. Chem. Phys.* **31**, 688–699.

Calderer, M. C. & Shen, Q. 2002 Axisymmetric configurations of bipolar liquid crystal droplets. *Continuum Mech. Thermodyn.* **14**, 363–375.

Canuto, C., Hussaini, M. Y., Quarteroni, A. & Zang, T. A. 1987 *Spectral Methods in Fluid Dynamics*. Springer.

Chang, Y. C., Hou, T. Y., Merriman, B. & Osher, S. 1996 A level set formulation of Eulerian interface capturing methods for incompressible fluid flows. *J. Comput. Phys.* **124**, 449–464.

Chen, L. Q. & Shen, J. 1998 Applications of semi-implicit Fourier-spectral method to phase field equations. *Comput. Phys. Commun.* **108**, 147–158.

Chuang, T.-K. & Flumerfelt, R. W. 1997 Dual optical monitoring of axisymmetric thin aqueous film drainage. *Rev. Sci. Instrum.* **68**, 3839–3842.

Cristini, V., Blawzdziewicz, J. & Loewenberg, M. 1998 Drop breakup in three-dimensional viscous flows. *Phys. Fluids* **10**, 1781–1783.

Doi, M. & Edwards, S. F. 1986 *The Theory of Polymer Dynamics*. Oxford University Press.

Ericksen, J. L. 1991 Liquid crystals with variable degree of orientation. *Arch. Rat. Mech. Anal.* **113** 97–120.

Feng, J., Sgalari, G. & Leal, L. G. 2000 A theory for flowing nematic polymers with orientational distortion. *J. Rheol.* **44**, 1085–1101.

de Gennes, P. G. 1980 Dynamics of fluctuations and spinodal decomposition in polymer blends. *J. Chem. Phys.* **72**, 4756–4763.

de Gennes, P. G. & Prost, J. 1993 *The Physics of Liquid Crystals*, 2nd Edn, Oxford University Press.

Gliklikh, Y. 1997 *Global Analysis in Mathematical Physics: Geometric and Stochastic Methods*. Springer.

de Groot, S. R. & Mazur, P. 1962 *Nonequilibrium Thermodynamics*. North-Holland.

Hohenberg, P. C. & Halperin, B. I. 1977 Theory of dynamic critical phenomena. *Rev. Mod. Phys.* **49**, 435–479.

Hooper R., Toose, M., Macosko, C. W. & Derby, J. J. 2001*a* A comparison of boundary element and finite element methods for modeling axisymmetric polymeric drop deformation. *Intl. J. Numer. Meth. Fluids* **37**, 837–864.

Hooper R. W., de Almeida V. F., Macosko C. W. & Derby J. J. 2001*b* Transient polymeric drop extension and retraction in uniaxial extensional flows. *J. Non-Newtonian Fluid Mech.* **98**, 141–168.

Hu, H. H., Patankar, N. A. & Zhu, M. Y. 2001 Direct numerical simulations of fluid-solid systems using the arbitrary Lagrangian-Eulerian technique. *J. Comput. Phys.* **169**, 427–462.

Huang, W. & Tuthill, G. F. 1994 Structure and shape of nematic liquid-crystal microdroplets. *Phys. Rev.* E **49**, 570–574.

Jacqmin, D. 1999 Calculation of two-phase Navier-Stokes flows using phase-field modelling. *J. Comput. Phys.* **155**, 96–127.

Jacqmin, D. 2000 Contact-line dynamics of a diffuse fluid interface. *J. Fluid. Mech.* **402**, 57–88.

Khayat, R. E. 2000 Three-dimensional boundary-element analysis of drop deformation for Newtonian and viscoelastic systems. *Intl J. Numer. Meth. Fluids* **34**, 241–275.

Kim, S. J. & Han, C. D. 2001 Finite element analysis of axisymmetric creeping motion of a deformable non-Newtonian drop in the entrance region of a cylindrical tube. *J. Rheol.* **45**, 1279–1303.

Lapeña, A. M., Glotzer, S. C., Langer, S. A. & Liu, A. J. 1999 Effect of ordering on spinodal decomposition of liquid-crystal/polymer mixtures. *Phys. Rev.* E **60**, R29–R32.

Larson, R. G. 1999 *The Structure and Rheology of Complex Fluids*. Oxford University Press.

Li, J. & Renardy, Y. 2000*a* Numerical study of flows of two immiscible liquids at low Reynolds number. *SIAM Rev.* **42**, 417–439.

Li, J. & Renardy, Y. 2000*b* Shear-induced rupturing of a viscous drop in a Bingham liquid. *J. Non-Newtonian Fluid Mech.* **95**, 235–251.

Lin, F. H. & Liu, C. 1995 Nonparabolic dissipative systems, modeling the flow of liquid crystals. *Commun. Pure Appl. Maths* **48**, 501–537.

Lin, F. H. & Liu, C. 2000 Existence of solutions for the Ericksen-Leslie system. *Arch. Rat. Mech. Anal.* **154**, 135–156.

Liu, C. & Shen, J. 2003 A phase field model for the mixture of two incompressible fluids and its approximation by a Fourier-spectral method. *Physica* D **179**, 211–228.

Liu, C. & Walkington, N. J. 2000 Approximation of liquid crystal flows. *SIAM J. Numer. Anal.* **37**, 725–741.

Liu, C. & Walkington, N. J. 2002 Mixed methods for the approximation of liquid crystal flows. *Math. Modeling Numer. Anal.* **36**, 205–222.

Lowengrub, J. & Truskinovsky, L. 1998 Quasi-incompressible Cahn-Hilliard fluids and topological transitions. *Proc. R. Soc. Lond.* A **454**, 2617–2654.

Maffettone, P. L. & Minale, M. 1998 Equation of change for ellipsoidal drops in viscous flow. *J. Non-Newtonian Fluid Mech.* **78**, 227–241.

Mauri, R., Shinnar, R. & Triantafyllou, G. 1996 Spinodal decomposition in binary mixtures. *Phys. Rev.* E **53**, 2613–2623.

Mo, H., Zhou, C. & Yu, W. 2000 A new method to determine interfacial tension from the retraction of ellipsoidal drops. *J. Non-Newtonian Fluid Mech.* **91**, 221–232.

National Research Council 1991 *Liquid Crystalline Polymers*. Washington, DC.

Nobari, M. R., Jan, Y.-J. & Tryggvason, G. 1996 Head-on collision of drops—a numerical investigation. *Phys. Fluids* **8**, 29–42.

Peskin, C. S. 1985 A random-walk interpretation of the incompressible Navier-Stokes equations. *Commun. Pure Appl. Maths* **38**, 845–852.

Pillapakkam, S. B. & Singh, P. 2001 A level-set method for computing solutions to viscoelastic two-phase flow. *J. Comput. Phys.* **174**, 552–578.

Rallison, J. M. 1984 The deformation of small viscous drops and bubbles in shear flows. *Annu. Rev. Fluid Mech.* **16**, 45–66.

Ramaswamy, S. & Leal, L. G. 1999*a* The deformation of a viscoelastic drop subjected to steady uniaxial extensional flow of a Newtonian fluid. *J. Non-Newtonian Fluid Mech.* **85**, 127–163.

Ramaswamy, S. & Leal, L. G. 1999*b* The deformation of a Newtonian drop in the uniaxial extensional flow of a viscoelastic liquid *J. Non-Newtonian Fluid Mech.* **88**, 149–172.

Rapini, A. & Popoular, M. 1969 Distortion d'une lamelle nematique sous champ magnetique conditions d'ancrage aux parois. *J. Phys. Paris* C **30**, 54–56.

Rey, A. D. 2000 Viscoelastic theory for nematic interfaces. *Phys. Rev.* E **61**, 1540–1549.

Sethian, J. A. & Smereka, P. 2003 Level set methods for fluid interfaces. *Annu. Rev. Fluid Mech.* **35**, 341–372.

Shen, J. 1995 Efficient spectral-Galerkin method. II. Direct solvers of second and fourth order equations by using Chebyshev polynomials. *SIAM J. Sci. Comput.* **16**, 74–87.

Son, Y. & Yoon, J. T. 2001 Measurement of interfacial tension by a deformed drop retraction method. *Polymer* **42**, 7209–7213.

Stone, H. A. 1994 Dynamics of drop deformation and breakup in viscous fluids. *Annu. Rev. Fluid Mech.* **26**, 65–102.

Stone, H. A. & Leal, L. G. 1989 Relaxation and breakup of an initially extended drop in an otherwise quiescent fluid. *J. Fluid Mech.* **198**, 399–427.

Toose, E. M., Geurts, B. J. & Kuerten, J. G. M. 1995 A boundary integral method for two-dimensional (non)-Newtonian drops in slow viscous flow. *J. Non-Newtonian Fluid Mech.* **60**, 129–154.

Unverdi, S. O. & Tryggvason, G. 1992 A front-tracking method for viscous, incompressible, multi-fluid flows. *J. Comput. Phys.* **100**, 25–37.

Utracki, L. A. 1990 *Polymer Alloys and Blends*. Hanser.

Verschueren, M., van de Vosse, F. N. & Meijer, H. E. H. 2001 Diffuse-interface modelling of thermocapillary flow instabilities in a Hele-Shaw cell. *J. Fluid Mech.* **434**, 153–166.

van der Waals, J. D. 1892 The thermodynamic theory of capillarity under the hypothesis of a continuous variation of density. *Verhandel Konink. Akad. Weten. Amsterdam*, (Sect. 1) **1** (no. 8), 1–56 (in Dutch). Translation by J. S. Rowlingson, *J. Statist. Phys.* **20** (1979), 197–244.

Warren, J. A. & Boettinger, W. J. 1995 Prediction of dendritic growth and microsegregation patterns in a binary alloy using the phase-field method. *Acta Metall. Mater.* **43**, 689–703.

West, J. L. 1990 Polymer-dispersed liquid crystals. In *Liquid-Crystalline Polymers*, ACS Symp. Ser. 435 (ed. R. A. Weiss & C. K. Ober), Chap. 32.

Wu, J. & Mather, P. T. 2002 Interfacial tension in an immiscible blend containing a thermotropic liquid-crystalline polymer. Paper HS12, *Society of Rheology 74th Annual Meeting, Minneapolis, MN, USA.*

Yang, H., Park, C. C., Hu, Y. T. & Leal, L. G. 2001 The coalescence of two equal-sized drops in a two-dimensional linear flow. *Phys. Fluids* **13**, 1087–1106.

Yu, R., Yu, W., Zhou, C. & Feng, J. J. 2004 Dynamic interfacial properties between a flexible isotropic polymer and a TLCP investigated by an ellipsoidal drop retraction method. *J. Appl. Polymer Sci.* (accepted).

Zhou, H. & Pozrikidis, C. 1993 The flow of suspensions in channels: Single files of drops. *Phys. Fluids* A **5**, 311–324.